Resonant direct CNOT in remote double quantum dot spin qubits

Stephen R. McMillan ● and Guido Burkard ●
Department of Physics, University of Konstanz, Konstanz D-78457, Germany

A critical element towards the realization of scalable quantum processors is nonlocal coupling between nodes. Scaling connectivity beyond nearest-neighbor interactions requires the implementation of a mediating interaction often termed a quantum bus. Cavity photons have long been used as a bus by the superconducting qubit community, but it has only recently been demonstrated that spin-based qubits in double quantum dot architectures can reach the strong coupling regime and exhibit spin-spin interactions via the exchange of real or virtual photons. Two-qubit gate operations are predicted in the dispersive regime where cavity loss plays a less prominent role. In this work we combine a cross-resonance entangling drive with simultaneous local rotations to propose a framework for a resonant direct-CNOT operation, between two nonlocal single-spin qubits dispersively coupled to a common mode of a superconducting resonator. We expect gate times near 100 ns and fidelities above 90% with existing technology.

I. INTRODUCTION

Electron spins in quantum dots (QDs) have long been an attractive candidate for spin-based computation and information processing [1–3]. Spin initialization and readout has been demonstrated through spin-to-charge conversion [4,5], and remarkably long spin coherence times have been reached in Si-based QDs as a result of isotopic purification [6]. Additionally, the use of local magnetic field gradients allows for all-electric spin manipulation [7,8]. These milestones have lead to the recent realization of fault-tolerant single- and two-qubit gates [9–14]. With an eye on building quantum networks [15,16] and simulations [17], these single-qubit systems can be scaled by an order of magnitude through tunnel-coupled linear and two-dimensional arrays which demonstrate spin-coherent charge displacement [18–21]. These dense qubit arrays provide registers for implementation of surface code protocols, but interconnection of these registers will require some form of long-range coupling [16].

Achieving reliable long-range coupling in quantum systems is perhaps the most pressing obstacle to realizing the next generation of quantum technology. Extending beyond micron-scale intermediate coupling schemes [22,23] to macroscopic separations on the order of 1 mm requires coupling to an ancillary system [24,25], a so-called "quantum bus." Photonic coupling of superconducting qubits by way of superconducting resonators was realized well over a decade ago [26] alongside proposals for coupling QD qubits with superconducting circuits [27–29]. The relatively weak magnetic dipole coupling rate between a single photon and an electron is inherently too slow (10–500 Hz) to overcome dephasing or cavity loss, presenting a clear challenge to reaching the strong spin-photon coupling regime [30]. Theoretical proposals have been aimed at alleviating this issue by coupling the spin to the photon indirectly through the electric dipole moment [31]. Spin-charge hybridization along with the use of micromagnetics to establish local field gradients lead to the realization

of strong spin-photon coupling for single spins in Si-based double QDs (DQDs) [32,33].

Cavity-mediated spin-spin interactions have been realized in both the resonant [34] and the dispersive [35] regimes. Universal two-qubit photon-mediated gates are predicted to exist for DQD spin qubits [36,37], and driven two-qubit gates have been proposed for both superconducting qubits and quantum-dot spin qubits, such as the cross-resonance (CR) gate [38,39]. The essence of the cross-resonance gate is the conditional rotation of the target qubit based on the orientation of the control qubit. The fidelity of the CR gate can be enhanced by echoing the CR pulse [40] and applying rotary tones to the target qubit [39,41,42]. However, these optimized schemes still require additional local rotations on the target qubit to yield a CNOT gate. Performing these local rotations in series with the cross-resonance pulse can be suboptimal for circuit performance, and in superconducting platforms applying the local rotations in parallel with the CR pulse, the so-called "direct-CNOT," is shown to be an essential ingredient in building circuits with larger quantum volume [43].

In this article, we propose a framework for realizing a direct-CNOT gate between two single-electron DQD qubits dispersively coupled to a common cavity mode. By tuning the spin-charge hybridization these spin qubits are predicted to outperform their charge qubit counterpart [36]. Here we show that driving both spins at a common frequency and asymmetric amplitudes allows for controlled two-qubit rotations. We expect synchronization of the drive strength to produce a high-fidelity direct-CNOT gate within the entanglement time of the CR scheme, similar to direct-CNOT conditions in superconducting qubits [44]. These gate times can rival those predicted for local operations on driven exchange-coupled spin qubits [45]. Given the sensitivity of QD spin qubits to local nuclei, gate fidelity should benefit from isotopically purified ^{28}Si, where even in the presence of cavity loss and phonon emission fidelities larger than 90% should be possible.
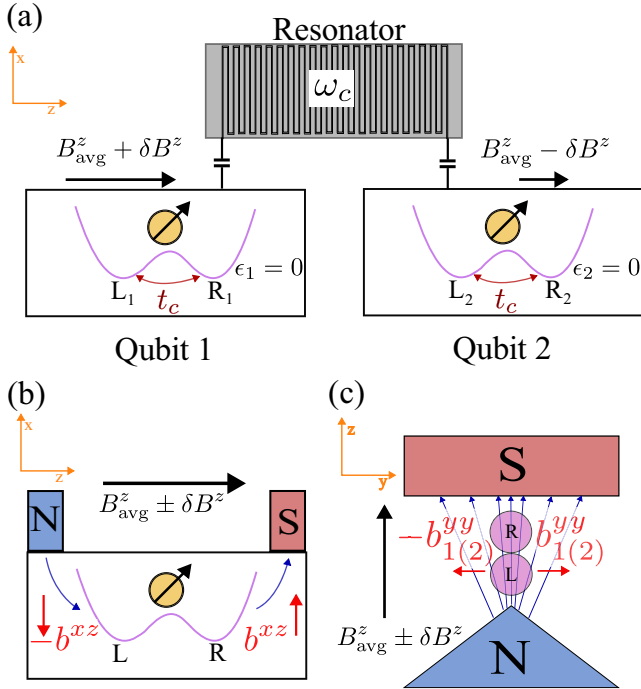
FIG. 1. (a) Diagram of the system. Two symmetric flopping-mode spin qubits with tunnel coupling t_c are coupled to the same cavity mode of a microwave resonator. A gradient between the external field at qubit 1 (B_1^z) and qubit 2 (B_2^z), $\delta B^z = B_2^z - B_1^z$ [$B_{avg}^z = (B_1^z + B_2^z)/2$], lifts the degeneracy between antiparallel spin configurations, allowing the individual spins to be addressed. (b) View along the y axis of a longitudinal field gradient in the x component of the field, b^{xz}, which provides an artificial spin-orbit coupling, allowing the spin to couple to the photon through the electric dipole of the DQD. This gradient is assumed to be equal for DQD1 and DQD2. (c) View along the x axis of local transverse gradients in the y component of the field, b_j^{yy}, which provide an electrically driven ac magnetic field used to drive spin transitions. Gradients of this type could result from the diverging field lines of a pointed micromagnet at the surface of the device, as shown in the cartoon.

II. MODEL

We consider two singly charged DQDs capacitively coupled to a common mode of a superconducting microwave resonator (cavity) with frequency ω_c, as sketched in Fig. 1(a). The energy detuning between the right (R) and left (L) dots, ϵ, and the tunnel coupling t_c are electrically controlled, and the spin-photon interaction is facilitated by a local inhomogeneous magnetic field, $\partial B^x / \partial z$. We assume the gradient to be linear with the difference in field between the two dots parametrized by the quantity $b_j^{xz} = [B_j^x(R_j) - B_j^x(L_j)]/2$, where j indicates the DQD. For simplicity we take this local gradient at the first DQD to be equal to that at the second DQD, i.e., $b_1^{xz} = b_2^{xz} = b^{xz}$, as depicted in Fig. 1(b). We set $\hbar = 1$ and begin in the double-dot basis by considering the model Hamiltonian $\tilde{H} = \tilde{H}_0 + \tilde{H}_d(t) + \tilde{H}_I$, with $\tilde{H}_0 = \sum_j (t_c \tilde{\tau}_j^x + \epsilon_j \tilde{\tau}_j^z)/2 + B_j^z \tilde{\sigma}_j^z / 2 + b^{xz} \tilde{\tau}_j^z \tilde{\sigma}_j^x / 2) + \omega_c a^\dagger a$. In this expression, B_j^z is the external field, $a^\dagger$ (a) is the photonic creation (annihilation) operator, $\tilde{\sigma}_j^k$ for $k = \{x, y, z\}$ are the spin Pauli matrices, and $\tilde{\tau}_j^k$ for

$k = \{x, y, z\}$ are the spatial Pauli matrices satisfying the relation $\tau_j^z |L_j(R_j)\rangle = (-1)|L_j(R_j)\rangle$. The driving Hamiltonian is written as $\tilde{H}_d(t) = \sum_j b_j^{yy} \cos(\omega_j^d t + \phi) \tilde{\sigma}_j^y / 2$, where $b_j^{yy} = [B_j^y(y_{max}) - B_j^y(-y_{max})]/2$ is used to parametrize the linear gradient of the form $\partial B^y / \partial y$, and y_{max} represents the maximum displacement of the spin from equilibrium along the y axis. This gradient is used to drive the spin through electrically driven spin resonance with the driving frequency ω_j^d and the phase ϕ [7,8,32,33,46,47]. A cartoon representation of this gradient is shown in Fig. 1(c). The charge couples to the cavity mode through a dipolar interaction with the Hamiltonian $\tilde{H}_{int} = \sum_j g_c(a^\dagger + a) \tilde{\tau}_j^z$. The electric dipole coupling strength g_c is proportional to the dipole moment of the DQD and is therefore electrically controllable through ϵ. In what follows we maximize the dipole moment of the DQD by choosing the symmetric configuration where the charge is equally likely to be in the R or L dot ($\epsilon = 0$).

The tunnel coupling t_c hybridizes the double-dot states to form the symmetric and antisymmetric states $|\pm_j\rangle = (|L_j\rangle \pm |R_j\rangle)/\sqrt{2}$. These states hybridize with the spin due to the local gradient b_j^{xz}. Recasting the Hamiltonian in the basis of $\tilde{H}_0$ leads to the transformed components,

$$H_0 = \frac{1}{2} \sum_j \left(E_j^\tau \tau_j^z + E_j^\sigma \sigma_j^z \right) + \omega_c a^\dagger a,$$

$$H_d(t) = \frac{1}{2} \sum_j \left(D_j^\tau \tau_j^y \sigma_j^z + D_j^\sigma \sigma_j^y \right) \cos\left(\omega_j^d t + \phi \right),$$

$$H_I = \sum_j \left(g_j^\tau \tau_j^x - g_j^\sigma \sigma_j^x \tau_j^z \right) \left(a^\dagger + a \right), \quad (1)$$

where the driving strengths are $D_j^\sigma = b_j^{yy} \cos \bar{\theta}_j$ and $D_j^\tau = b_j^{yy} \sin \bar{\theta}_j$, and the cavity coupling strengths are $g_j^\sigma = g_c \sin \bar{\theta}_j$ and $g_j^\tau = g_c \cos \bar{\theta}_j$ for spin and charge, respectively. These terms depend on the average hybridization angle $\bar{\theta}_j = (\theta_j^+ + \theta_j^-)/2$, where $\theta_j^\pm = \arctan[b^{xz}/(2t_c \pm B_j^z)] \in [0, \pi]$. In what follows, we assume $2t_c > B_j^z \gg b^{xz}$, in analogy to Ref. [36]. The charge (spin) transition energies are then given by $E_j^{\tau(\sigma)} = E_{2(1),j} - E_{0,j}$, where $E_{2(1),j} = \pm \sqrt{(2t_c - B_j^z)^2 + (b^{xz})^2}/2$ and $E_{0,j} = -\sqrt{(2t_c + B_j^z)^2 + (b^{xz})^2}/2$.

Dispersive coupling between the DQDs and the cavity mitigates losses due to interactions with real photons, limiting the spin-photon exchange to short-lived virtual transitions [35,48]. The dispersive regime requires the cavity frequency to be detuned from the spin transition energy by the amount $\Delta_j = E_j^\sigma - \omega_c$ such that $\Delta_j \gg g_j^\sigma$. In this regime the photonic states are weakly coupled, and we perform a Schrieffer-Wolff transformation to decouple the vacuum state from the populated photon states up to first order in the perturbative parameters $g_{\tau(\sigma)}/|E_{\tau(\sigma)} - \omega_c|$ [36]:

$$\mathcal{H}^d = \sum_j \left(\tilde{E}_j^\tau \tau_j^z + \tilde{E}_j^\sigma \sigma_j^z + \left(D_j^\tau \tau_j^y \sigma_j^z + D_j^\sigma \sigma_j^y \right) \right.$$

$$\times \cos\left(\omega_j^d t + \phi \right)/2 + S_j^x \sigma_j^x \tau_j^x + S_j^y \sigma_j^y \tau_j^y \right)$$

$$+ J^\tau \tau_1^x \tau_2^x - J^{\sigma 1, \tau 2} \sigma_1^x \tau_1^z \tau_2^x$$

$$- J^{\sigma 2, \tau 1} \tau_1^x \sigma_2^x \tau_2^z + \mathcal{J} \sigma_1^x \sigma_2^x \tau_1^z \tau_2^z, \quad (2)$$

where the Pauli matrices σ_j^k and τ_j^k now correspond to the qubits dressed by the photonic excitations. The dressed energy levels are $\tilde{E}_j^\sigma = \frac{1}{2}[E_j^\sigma + 2(g_j^\sigma)^2 \frac{E_j^\sigma}{(E_j^\sigma)^2 - \omega_c^2}]$ and $\tilde{E}_j^\tau = \frac{1}{2}[E_j^\tau + 2(g_j^\tau)^2 \frac{E_j^\tau}{(E_j^\tau)^2 - \omega_c^2}]$, the local spin-charge coupling coefficients are $S_j^x = g_j^\sigma g_j^\tau \frac{E_j^\tau}{(E_j^\tau)^2 - \omega_c^2}$ and $S_j^y = g_j^\sigma g_j^\tau \frac{E_j^\sigma}{(E_j^\sigma)^2 - \omega_c^2}$, the nonlocal charge-charge coupling coefficient is $J^\tau = g_1^\tau g_2^\tau \omega_c [\frac{1}{(E_1^\tau)^2 - \omega_c^2} + \frac{1}{(E_2^\tau)^2 - \omega_c^2}]$, the nonlocal spin-spin coupling coefficient is $\mathcal{J} = g_1^\sigma g_2^\sigma \omega_c [\frac{1}{(E_1^\sigma)^2 - \omega_c^2} + \frac{1}{(E_2^\sigma)^2 - \omega_c^2}]$, and the nonlocal spin-charge coefficients are $J^{\sigma 1(2), \tau 2(1)} = g_{1(2)}^\sigma g_{2(1)}^\tau \omega_c [\frac{1}{(E_{1(2)}^\sigma)^2 - \omega_c^2} + \frac{1}{(E_{2(1)}^\tau)^2 - \omega_c^2}]$. Tuning the cavity frequency such that $g_j^\tau \Delta_j / |E_j^\tau - \omega_c| \ll g_j^\sigma \ll \Delta_j$ is the most interesting for spin-qubit operation [36]. In the rotating-wave approximation the dispersive Hamiltonian can be approximated as

$$\mathcal{H}^d \approx \sum_j \left[\tilde{E}_{\text{avg}}^\sigma \sigma_j^z + i D_j^\sigma \left(e^{i(\omega_j^d t + \phi_j)} \sigma_j^- - e^{-i(\omega_j^d t + \phi_j)} \sigma_j^+ \right)/4 \right]$$
$$+ \frac{1}{2} \delta\tilde{E}^\sigma \left(\sigma_1^z - \sigma_2^z \right) + \frac{\mathcal{J}}{2} \left(\sigma_1^+ \sigma_2^- + \sigma_1^- \sigma_2^+ \right), \quad (3)$$

where $\sigma_j^{+(-)}$ is the spin-raising(lowering) operator of the jth qubit. The cavity-mediated spin-spin interaction coefficient simplifies to $\mathcal{J} \approx g_1^\sigma g_2^\sigma (\frac{1}{\Delta_1} + \frac{1}{\Delta_2})$ when $E_j^\sigma \sim \omega_c$. Due to the difference in external field between the two qubits, the dressed energy levels have been written in terms of an average spin-flip energy, $\tilde{E}_{\text{avg}}^\sigma = (\tilde{E}_1^\sigma + \tilde{E}_2^\sigma)/2$, and a difference term, $\delta\tilde{E}^\sigma = \tilde{E}_1^\sigma - \tilde{E}_2^\sigma$. Since the cavity is tuned closer to the spin transition energy, any nonlocal charge-charge and spin-charge transitions are highly off-resonant and therefore provide a negligible contribution to the dynamics. Additionally, by tuning the local driving to spin transitions, the local charge transitions are negligible for the same reason, and the resulting Hamiltonian has no relevant dynamics in the charge channel. We therefore take the computational subspace to be the lowest energy charge sector.

We now assume that both spins are driven at the same frequency ($\omega_1^d = \omega_2^d = \omega^d$), but not necessarily the same strength. This allows one to drive entanglement in addition to local rotations. Next we assume the spin-spin interaction to be small relative to the spin-flip gradient, $\mathcal{J} \ll \delta\tilde{E}^\sigma$, and we use the adiabatic basis, $\{|\uparrow\uparrow\rangle, \widetilde{|\downarrow\uparrow\rangle}, \widetilde{|\uparrow\downarrow\rangle}, |\downarrow\downarrow\rangle\}$, where $\mathcal{H}$ is diagonalized with respect to the spin-spin interaction. The weak spin-spin interaction slightly hybridizes the antiparallel product states $\widetilde{|\uparrow\downarrow\rangle} = \cos(\xi/2)|\uparrow\downarrow\rangle + \sin(\xi/2)|\downarrow\uparrow\rangle$ and $\widetilde{|\downarrow\uparrow\rangle} = -\sin(\xi/2)|\uparrow\downarrow\rangle + \cos(\xi/2)|\downarrow\uparrow\rangle$ with the hybridization angle $\xi = \arctan(\mathcal{J}/2\delta\tilde{E}^\sigma) \in [0, \pi]$. In this basis the only off-diagonal contribution comes from the driving term, which can be written as

$$\hat{\mathcal{H}}_d(t) = \frac{D_1^\sigma}{2} \cos(\omega^d t + \phi) \left[\cos(\xi/2)\hat{\sigma}_1^y + \sin(\xi/2)\hat{\sigma}_1^z \hat{\sigma}_2^y \right]$$
$$+ \frac{D_2^\sigma}{2} \cos(\omega^d t + \phi) \left[\cos(\xi/2)\hat{\sigma}_2^y - \sin(\xi/2)\hat{\sigma}_1^y \hat{\sigma}_2^z \right]. \quad (4)$$

In order to illuminate the choice to drive at a common frequency, consider DQD1 to be the *target* qubit and DQD2 to be the *control* qubit. Driving the two qubits at the resonant
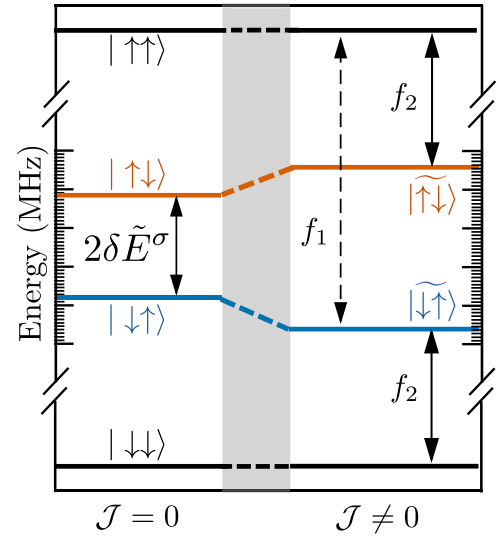

FIG. 2. Sketch of the energy levels for the spin manifold in the lowest charge sector. A gradient in the external field lifts the degeneracy between the $m_s = 0$ states. Once the cavity-mediated spin-spin interaction is present the $m_s = 0$ levels experience an additional symmetric shift in frequency. Frequency f_1 (f_2) drives the spin at DQD1(2) unconditionally due to the symmetry of the system.

frequency of DQD1 reduces Eq. (4) to

$$\hat{\mathcal{H}}_d(t) \approx \frac{1}{2} D_1^\sigma \cos\left(\omega^d t + \phi\right) \cos(\xi/2)\hat{\sigma}_1^y$$
$$- \frac{1}{2} D_2^\sigma \cos(\omega^d t + \phi) \sin(\xi/2)\hat{\sigma}_1^y \hat{\sigma}_2^z. \quad (5)$$

The first term in Eq. (5) describes a local rotation of the target while the second describes the entangling CR term. The objective is to synchronize these terms in such a way that the pulses result in a direct-CNOT gate.

Figure 2 shows a sketch of the energy levels for states in the computational subspace. The effective gradient in the external field, $\delta\tilde{E}^\sigma$, lifts the degeneracy between the $m_s = 0$ states. The presence of the nonlocal spin-spin coupling adds an additional symmetric frequency shift to the $m_s = 0$ states in the adiabatic basis. This symmetric splitting is in contrast to the uniform shift seen for homogeneous exchange coupling [45] which allows for direct access to conditional rotations. The symmetry of *this* system dictates that frequency f_1 (f_2) resonantly drives the spin at DQD1(2) regardless of the spin orientation at DQD2(1). The primary aim of this work is to synchronize D_1^σ and D_2^σ in order to generate conditional rotations of the target qubit. To eliminate the time dependence in Eq. (4), we work in a frame rotating at the drive frequency about the spin quantization axis. The rotating-frame Hamiltonian has the form $\mathring{\mathcal{H}} = i\dot{\hat{R}}(t)\hat{R}^\dagger(t) + \hat{R}(t)\hat{\mathcal{H}}(t)\hat{R}^\dagger(t)$, where $\hat{R} = \exp[i\omega^d(\hat{\sigma}_1^z + \hat{\sigma}_2^z)t/2]$. The time-independent Hamiltonian can be expressed as

$$\mathring{\mathcal{H}} = \begin{pmatrix} \lambda_\parallel & -i\alpha_-^* & -i\beta_+^* & 0 \\ i\alpha_- & -\lambda_\perp & 0 & -i\beta_-^* \\ i\beta_+ & 0 & \lambda_\perp & -i\alpha_+^* \\ 0 & i\beta_- & i\alpha_+ & -\lambda_\parallel \end{pmatrix}, \quad (6)$$

with $\lambda_\parallel = 2\tilde{E}^\sigma_{\mathrm{avg}} - \omega^d$, $\lambda_\perp = \sqrt{(\delta\tilde{E}^\sigma)^2 + (\mathcal{J}/2)^2}$, and the effective driving amplitudes

$$\alpha_\pm = \tfrac{1}{4}\big[\pm\sin(\xi/2)D^\sigma_2 + \cos(\xi/2)D^\sigma_1\big]e^{i\phi} \qquad (7)$$

and

$$\beta_\pm = \tfrac{1}{4}\big[\pm\sin(\xi/2)D^\sigma_1 + \cos(\xi/2)D^\sigma_2\big]e^{i\phi}. \qquad (8)$$

In what follows we rely on the hybridized driving amplitudes to generate a single-shot CNOT gate.

III. RESONANT NONLOCAL DIRECT-CNOT GATE

For a CNOT gate we define the spin in DQD1 to be the target and the spin in DQD2 to be the control, as previously discussed. Using the same basis as in Eq. (6), this operation is represented by the matrix

$$U_{\mathrm{CNOT}} = \begin{pmatrix} 0 & 1 & 0 & 0 \\ 1 & 0 & 0 & 0 \\ 0 & 0 & 1 & 0 \\ 0 & 0 & 0 & 1 \end{pmatrix}. \qquad (9)$$

To model this operation we require the target spin to flip if the control is spin-up and an identity operation if the control is spin-down. To resonantly drive the spin at DQD1 we choose a driving frequency that is determined by the energy separation between $|\uparrow\uparrow\rangle$ and $|\widetilde{\downarrow\uparrow}\rangle$: $\omega^d - \delta\omega^d = \lambda_\parallel + \lambda_\perp$, where $\delta\omega^d$ accounts for the detuning between the drive and the energy separation between the two levels. On resonance, $\delta\omega^d = 0$, the β transitions couple states split in energy by the relatively large quantity $2\delta\tilde{E}^\sigma$. As long as the off-resonant transitions are weakly coupled ($\beta_\pm \ll \delta\tilde{E}^\sigma$) the Hamiltonian expressed in Eq. (6) is effectively block diagonal, with both $\{|\uparrow\uparrow\rangle, |\widetilde{\downarrow\uparrow}\rangle\}$ and $\{|\widetilde{\uparrow\downarrow}\rangle, |\downarrow\downarrow\rangle\}$ blocks producing full Rabi oscillations at frequencies $\Omega_- = 2|\alpha_-|$ and $\Omega_+ = 2|\alpha_+|$, respectively. The time required for maximum population transfer between the states $|\uparrow\uparrow\rangle \leftrightarrow |\widetilde{\downarrow\uparrow}\rangle$ is $t_{\mathrm{CNOT}} = (2m + 1)\pi/\Omega_-$, for integer m.

Treating the resonant blocks individually, we calculate the unitary operator for each. With the aim of obtaining the unitary in Eq. (9), the drive phase should be set such that the rotation is about the $\pm x$ axis: $\phi = (2\ell + 1)\pi/2$, for integer ℓ. Under this condition, the control spin-up block evolves as

$$U_{2=\uparrow} = e^{-i\mathcal{F}_1 t}\left[\cos\left(\frac{\Omega_- t}{2}\right)\mathbb{1} + i^{2\ell+1}\sin\left(\frac{\Omega_- t}{2}\right)\sigma^x\right], \quad (10)$$

and the block for control spin-down evolves as

$$U_{2=\downarrow} = e^{-i\mathcal{F}_2 t}\left[\cos\left(\frac{\Omega_+ t}{2}\right)\mathbb{1} + i^{2\ell+1}\sin\left(\frac{\Omega_+ t}{2}\right)\sigma^x\right]. \quad (11)$$

The dynamic phase is dependent on the energy of the corresponding block, $\mathcal{F}_{1(2)} = \mp\sqrt{(\delta\tilde{E}^\sigma)^2 + (\mathcal{J}/2)^2}$. The choice of phase allows one to write the total unitary ($U = U_{2=\downarrow} \oplus U_{2=\uparrow}$) in the form of the CNOT unitary shown in Eq. (9), up to local rotations about the z axis. However, one could generate a conditional rotation about any arbitrary axis in the x-y plane by making the substitution $\sigma^x \to \sin\phi\,\sigma^x + \cos\phi\,\sigma^y$.

In order to generate a single-shot conditional rotation of the target spin, the Rabi frequencies Ω_+ and Ω_- should be out of
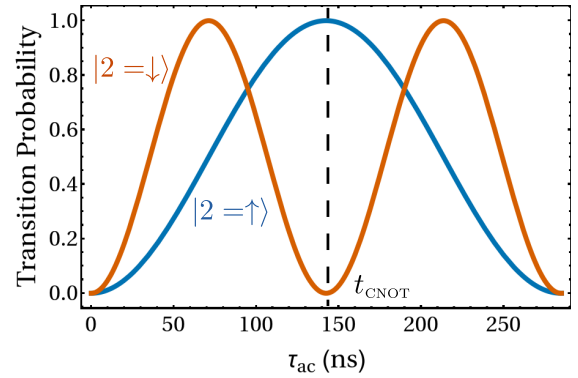

FIG. 3. Calculated transition probabilities for the synchronized $|2=\uparrow\rangle$ (blue) and $|2=\downarrow\rangle$ (red) blocks. The relevant parameters are chosen to be experimentally realizable with a driving strength $D^\sigma_2 = 100$ MHz. The integers $m = 0$ and $n = 1$ are chosen to minimize the gate time, shown here to be $t_{\mathrm{CNOT}} = 142$ ns. Parameters: $t_c = 3.6$ GHz, $B^z_{\mathrm{avg}} = 6.3$ GHz, $\delta B^z = 300$ MHz, $b^{xz} = 780$ MHz, $\omega_c = 5.6$ GHz, $g_c = 190$ MHz.

phase. The necessary condition is then

$$\Omega_- = \frac{2m+1}{2n}\Omega_+, \qquad (12)$$

with integer n. This can be done by adjusting the ratio of the ac driving strengths such that

$$\frac{D^\sigma_1}{D^\sigma_2} = -\frac{1 + 2(m+n)}{1 + 2(m-n)}\tan(\xi/2), \qquad (13)$$

where m and n obey Eq. (12). The unitary operator up to a global phase at time t_{CNOT} is

$$U(t_{\mathrm{CNOT}}) = e^{i(\Phi_{\mathrm{dyn}}+\Phi_{\mathrm{hol}})\sigma^z_2}U_{\mathrm{CNOT}}. \qquad (14)$$

The time-dependent dynamic phase is $\Phi_{\mathrm{dyn}} = \frac{\mathcal{F}_2 - \mathcal{F}_1}{2}t_{\mathrm{CNOT}}$ and the time-independent holonomic phase is $\Phi_{\mathrm{hol}} = \frac{\pi}{2}[(2\ell + 1)/2 + m - n]$.

Figure 3 shows the synchronized Rabi oscillations for the driven CNOT gate. System parameters were chosen to represent realistic experimental conditions and are quoted in the figure caption. The analytic expressions derived above for the unitary evolution ignore the off-resonant transitions with coupling $\beta_\pm$ in Eq. (6). In general, strong driving will increase population transfer through the off-resonant channels impacting the coherent average gate fidelity $\bar{F}_c$. Numerical calculations of this fidelity show that for a modest synchronized drive strength of $D^\sigma_2 = 100$ MHz we predict gate times of $t_{\mathrm{CNOT}} = 142$ ns with coherent average fidelity $\bar{F}_c = 0.99$. In principle, driving with this strength requires a field gradient with magnitude near 3.5 mT, a requirement well within the typical strength of contemporary micromagnetics ($\sim$1 mT/nm).

IV. DISCUSSION AND SUMMARY

In addition to the parasitic effects of off-resonant channels, coupling to the environment also reduces the fidelity of the gate. Since the spin qubit couples to the cavity through a virtual charge qubit, the gate is vulnerable to both

electron-phonon interaction and photonic loss through the cavity. However, since the charge qubit and photons are both virtual, the influence on gate fidelity is less pronounced than it would be under resonant coupling. To estimate these effects we calculate the average fidelity [49] in the presence of cavity loss, electron-phonon coupling, and general spin decoherence. The master equation in the dispersive basis follows the derivation from Ref. [36] and has the form

$$
\frac{d}{dt}\rho(t) = -i[\mathcal{H}^{\mathrm{d}}(t), \rho(t)] + \frac{\kappa}{2}\sum_j \frac{\left(g_j^\sigma\right)^2}{\Delta_j^2}\mathcal{D}[\sigma_j^-]\rho(t) + \sum_j \frac{\gamma_p^{E_j^\sigma}}{2}\sin^2\bar\theta_j \mathcal{D}\left[\left(1 - \frac{\left(g_j^\sigma\right)^2}{2\Delta_j^2}\right)\tau_j^z\sigma_j^-\right]\rho(t)
$$

$$
+ \sum_j \frac{\gamma_p^{E_j^\tau}}{2}\cos^2\bar\theta_j \mathcal{D}\left[\left(1 - \frac{\left(g_j^\sigma\right)^2}{\Delta_j^2}\right)\tau_j^- - \frac{\left(g_j^\sigma\right)^2}{\Delta_j^2}\tau_j^-\sigma_j^z\right]\rho(t)
$$

$$
+ 2\sum_j \gamma_p^{E_j^\tau + E_j^\sigma - \omega_c}\frac{\left(g_j^\sigma\right)^2}{\Delta_j^2}\frac{\left(E_j^\tau - E_j^\sigma\right)^2\cos^2\bar\theta_j}{\left(E_j^\tau - \omega_c\right)^2}\mathcal{D}[\tau_j^-\sigma_j^-]\rho(t) + \frac{\nu_{T_2^*}}{2}\sum_j \mathcal{D}[\sigma_j^z]\rho(t), \tag{15}
$$

where $\mathcal{D}[\hat o]$ represents the Lindblad superoperator $\mathcal{D}[\hat o]\rho = 2\hat o\rho\hat o^\dagger - \{\hat o^\dagger\hat o, \rho\}$, and $\{...\}$ represents the anticommutator. The density matrix $\hat\rho$ corresponds to the 16-dimensional spin-charge subspace for an empty cavity in the dispersive basis, and we assume the environment to be at zero temperature. The first term describes the coherent evolution of the system and the second term describes loss through the cavity at rate κ. Terms three, four, and five account for the relaxation due to electron-phonon coupling with rate γ_p^E at energy E, and the last term expresses general dephasing of the spin at rate $\nu_{T_2^*}$. In the following calculations we assume $\gamma_p^E = \gamma_p^{\omega_c}(E/\omega_c)^5$ [50].

An average measure of how well a trace-preserving quantum operation, $\mathcal{E}$, approximates a quantum gate, U, is defined as $\bar F(\mathcal{E}, U) \equiv \int d\psi \langle\psi|U^\dagger\mathcal{E}(\psi)U|\psi\rangle$. Making use of the entanglement fidelity [51], F_e, we calculate the average fidelity on the four-dimensional computational subspace spanned by the spin states in the lowest charge sector and an empty cavity. The evolution defined by Eq. (15) represents a trace nonpreserving map $\mathcal{E}'$ in this subspace and the expression for the average fidelity is given by [49,52] $\bar F(\mathcal{E}, U) = (\sum_j \mathrm{Tr}[UU_j^\dagger U^\dagger\mathcal{E}'(U_j)] + 16\mathrm{Tr}[\mathcal{E}'(\mathbb{1}/4)])/80$, where U represents the ideal unitary from Eq. (14) with a general control qubit phase, ζ. In the gate frame the generalized unitary has the form $U_{\mathrm{ideal}} = \exp(-i\zeta\sigma_2^z)U_{\mathrm{CNOT}}$, where ζ is chosen to numerically maximize the quantity $\sum_j \mathrm{Tr}[UU_j^\dagger U^\dagger\mathcal{E}'(U_j)]$. We also introduce a basis of unitary operators, $U_j = X^kZ^l$, on the four-dimensional two-qubit subspace, where $X|j\rangle = |j \oplus 1\rangle$ and $Z|j\rangle = e^{2\pi ij/4}|j\rangle$ are defined on computational basis states $|0\rangle, \dots, |3\rangle$. Here the operation $\oplus$ represents addition modulo 4.

Spin relaxation rates will depend on the degree of spin-charge hybridization, quantified by the angle $\bar\theta_j$. The degree of hybridization is determined by the local gradient b^{xz}, the tunnel coupling t_c, and the applied fields $B_{\mathrm{avg}}^z \pm \delta B^z$. In practice, the applied fields and field gradients are difficult to tune once set, but the tunnel coupling can be adjusted electrically through gate voltages.

In Fig. 4(a) we show the average fidelity as a function of the tunnel coupling within the range $B_{\mathrm{avg}}^z + \delta B^z \lesssim 2t_c$ for a synchronized drive strength of $D_{2,\mathrm{sync}}^\sigma = 150$ MHz which satisfies Eq. (13) with $m = 0$ and $n = 1$. The points indicate numerical solutions to Eq. (15) with $\kappa = 1.5$ MHz, $\gamma_p^{\omega_c} = 1$ MHz, and $\nu_{T_2^*} = 100$ kHz. The solid line shows a moving average in

order to capture the trend. As the tunnel coupling increases, the spin-charge hybridization decreases. This mitigates the
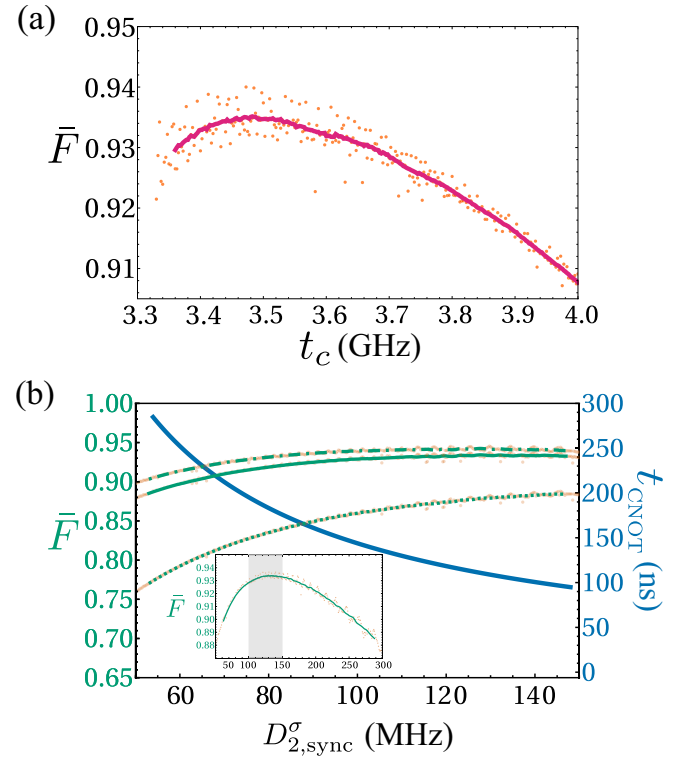

FIG. 4. (a) The average fidelity as a function of spin-charge hybridization via the tunnel coupling t_c for drive strength $D_{2,\mathrm{sync}}^\sigma = 150$ MHz, $\gamma_p^{\omega_c} = 1$ MHz, and $\nu_{T_2^*} = 100$ kHz. (b) The gate time and average fidelity as a function of synchronized drive strength for $\nu_{T_2^*} = 100$ kHz with $\gamma_p^{\omega_c} = 4$ MHz (green dotted) and $\gamma_p^{\omega_c} = 1$ MHz (green solid), and $\nu_{T_2^*} = 50$ kHz for $\gamma_p^{\omega_c} = 1$ MHz (green dot-dashed). The inset shows the fidelity for $\nu_{T_2^*} = 100$ kHz and $\gamma_p^{\omega_c} = 1$ MHz for a larger range of driving strengths to illustrate the impact of coherent off-resonant processes. Optimal strengths are indicated by the gray shaded region. In both (a) and (b) the orange points indicate the average fidelity found through numerical solutions of Eq. (15) and the overlaid lines represent a moving average. Additional parameters: $t_c = 3.6$ GHz, $B_{\mathrm{avg}}^z = 6.3$ GHz, $\delta B^z = 300$ MHz, $b^{xz} = 780$ MHz, $\omega_c = 5.6$ GHz, $g_c = 190$ MHz, $\kappa = 1.5$ MHz, $m = 0$, and $n = 1$.

coupling to phonons and cavity loss, but also reduces the magnitude of the spin-spin interaction. An optimal range is found between $t_c = 3.4$ GHz and $t_c = 3.6$ GHz, and since we assume $\mathcal{J}/\delta\tilde{E}^\sigma \ll 1$ in the analytic derivation above, we chose $t_c = 3.6$ GHz for the results presented in this work. The average fidelity and gate time are plotted in Fig. 4(b) as a function of the synchronized drive strength $D^\sigma_{2,\text{sync}}$ for three sets of realistic parameters. Once again, the points result from numerically solving Eq. (15) and the overlaid green lines represent a moving average. Strong driving leads to faster gate times (shown by the blue line) at the cost of increased transitions through off-resonant channels, which ultimately impact gate fidelity (see inset). However, weaker driving requires the system to be highly coherent, and if the gate time is too long incoherent processes become significant and the fidelity again suffers.

Competition between off-resonant evolution and dissipation results in an optimal drive strength that maximizes gate fidelity. The optimal synchronized drive strengths for the set of parameters shown in Fig. 4(b) are within the range $D^\sigma_{2,\text{sync}} \approx 100$–150 MHz, indicated by the gray region of the inset. The top-end parameters yield an average fidelity of $\bar{F} = 0.94$, as shown by the green dot-dashed line. However, using rather conservative values [53,54] still yields an average fidelity just below 90% ($\bar{F} = 0.88$) as shown by the dotted green line.

In practice, the symmetric ($\epsilon = 0$) configuration will be avoided while the qubits are idle in order to prolong coherence. This is done by adiabatically transferring the spin from the symmetric configuration to the single-dot configuration—a process which can also result in error. Transitions between symmetric and asymmetric dot levels are akin to physically shuttling a spin from one dot to the other. Adiabatic transfer fidelity in silicon-based double dots is predicted to be quite high (~ 0.99) for systems with weak gradients and relatively large applied fields [55]. We consider this to be a minor correction to the total gate fidelity, and we have, therefore, omitted it in this work.

With recently achieved electric dipole coupling strengths $g_c \approx 190$ MHz using high-impedance resonators [35], we predict gate fidelities well above 90% in the presence of cavity loss, phonon emission, and spin dephasing with gate times around 100 ns. We note that these gate times, compared to typical CR gate times, are a result of the driving strength and improvements in parameters, such as the electric dipole coupling, since the bottleneck in this scheme is still the cross-resonance entanglement time.

A gate fidelity near 90% is significantly lower than fault tolerance thresholds [15], but as technology creeps toward error-corrected circuits, optimizing noisy intermediate-scale quantum gates allows one to execute deeper circuits *without* error correction [56]. Additionally, it is likely that methods such as entanglement purification can be applied to increase the fidelity of the direct-CNOT [57,58]. Along with single-spin operations this work elucidates the potential for all electrical remote entanglement in solid-state DQD spin qubits and enhances the prospects of these systems for quantum information processing.

[1] D. Loss and D. P. DiVincenzo, Quantum computation with quantum dots, Phys. Rev. A **57**, 120 (1998).

[2] R. Hanson, L. P. Kouwenhoven, J. R. Petta, S. Tarucha, and L. M. K. Vandersypen, Spins in few-electron quantum dots, Rev. Mod. Phys. **79**, 1217 (2007).

[3] G. Burkard, T. D. Ladd, A. Pan, J. M. Nichol, and J. R. Petta, Semiconductor spin qubits, Rev. Mod. Phys. **95**, 025003 (2023).

[4] K. Ono, D. G. Austing, Y. Tokura, and S. Tarucha, Current rectification by Pauli exclusion in a weakly coupled double quantum dot system, Science **297**, 1313 (2002).

[5] J. M. Elzerman, R. Hanson, L. H. W. Van Beveren, B. Witkamp, L. M. K. Vandersypen, and L. P. Kouwenhoven, Single-shot read-out of an individual electron spin in a quantum dot, Nature (London) **430**, 431 (2004).

[6] M. Veldhorst, J. C. C. Hwang, C. H. Yang, A. W. Leenstra, B. de Ronde, J. P. Dehollain, J. T. Muhonen, F. E. Hudson, K. M. Itoh, A. Morello, and A. S. Dzurak, An addressable quantum dot qubit with fault-tolerant control-fidelity, Nat. Nanotechnol. **9**, 981 (2014).

[7] Y. Tokura, W. G. van der Wiel, T. Obata, and S. Tarucha, Coherent Single Electron Spin Control in a Slanting Zeeman Field, Phys. Rev. Lett. **96**, 047202 (2006).

[8] M. Pioro-Ladrière, T. Obata, Y. Tokura, Y.-S. Shin, T. Kubo, K. Yoshida, T. Taniyama, and S. Tarucha, Electrically driven single-electron spin resonance in a slanting Zeeman field, Nat. Phys. **4**, 776 (2008).

[9] K. Takeda, J. Kamioka, T. Otsuka, J. Yoneda, T. Nakajima, M. R. Delbecq, S. Amaha, G. Allison, T. Kodera, S. Oda, and S. Tarucha, A fault-tolerant addressable spin qubit in a natural silicon quantum dot, Sci. Adv. **2**, e1600694 (2016).

[10] J. Yoneda, K. Takeda, T. Otsuka, T. Nakajima, M. R. Delbecq, G. Allison, T. Honda, T. Kodera, S. Oda, Y. Hoshi, N. Usami, K. M. Itoh, and S. Tarucha, A quantum-dot spin qubit with coherence limited by charge noise and fidelity higher than 99.9%, Nat. Nanotechnol. **13**, 102 (2018).

[11] A. R. Mills, C. R. Guinn, M. M. Feldman, A. J. Sigillito, M. J. Gullans, M. Rakher, J. Kerckhoff, C. A. C. Jackson, and J. R. Petta, High Fidelity State Preparation, Quantum Control, and Readout of an Isotopically Enriched Silicon Spin Qubit, Phys. Rev. Appl. **18**, 064028 (2022).

[12] X. Xue, M. Russ, N. Samkharadze, B. Undseth, A. Sammak, G. Scappucci, and L. M. K. Vandersypen, Quantum logic with spin qubits crossing the surface code threshold, Nature (London) **601**, 343 (2022).

[13] A. Noiri, K. Takeda, T. Nakajima, T. Kobayashi, A. Sammak, G. Scappucci, and S. Tarucha, Fast universal quantum gate above the fault-tolerance threshold in silicon, Nature (London) **601**, 338 (2022).

[14] A. R. Mills, C. R. Guinn, M. J. Gullans, A. J. Sigillito, M. M. Feldman, E. Nielsen, and J. R. Petta, Two-qubit silicon quantum processor with operation fidelity exceeding 99%, Sci. Adv. **8**, eabn5130 (2022).

[15] A. G. Fowler, M. Mariantoni, J. M. Martinis, and A. N. Cleland, Surface codes: Towards practical large-scale quantum computation, Phys. Rev. A **86**, 032324 (2012).

[16] L. M. K. Vandersypen, H. Bluhm, J. S. Clarke, A. S. Dzurak, R. Ishihara, A. Morello, D. J. Reilly, L. R. Schreiber, and M. Veldhorst, Interfacing spin qubits in quantum dots and donors-hot, dense, and coherent, NPJ Quantum Inf. **3**, 34 (2017).

[17] T. Byrnes, N. Y. Kim, K. Kusudo, and Y. Yamamoto, Quantum simulation of Fermi-Hubbard models in semiconductor quantum-dot arrays, Phys. Rev. B **78**, 075320 (2008).

[18] T. Fujita, T. A. Baart, C. Reichl, W. Wegscheider, and L. M. K. Vandersypen, Coherent shuttle of electron-spin states, npj Quantum Inf **3**, 22 (2017).

[19] H. Flentje, P.-A. Mortemousque, R. Thalineau, A. Ludwig, A. D. Wieck, C. Bäuerle, and T. Meunier, Coherent long-distance displacement of individual electron spins, Nat. Commun. **8**, 501 (2017).

[20] U. Mukhopadhyay, J. P. Dehollain, C. Reichl, W. Wegscheider, and L. M. K. Vandersypen, A 2×2 quantum dot array with controllable inter-dot tunnel couplings, Appl. Phys. Lett. **112**, 183505 (2018).

[21] P.-A. Mortemousque, E. Chanrion, B. Jadot, H. Flentje, A. Ludwig, A. D. Wieck, M. Urdampilleta, C. Bäuerle, and T. Meunier, Coherent control of individual electron spins in a two-dimensional quantum dot array, Nat. Nanotechnol. **16**, 296 (2021).

[22] F. Hassler, G. Catelani, and H. Bluhm, Exchange interaction of two spin qubits mediated by a superconductor, Phys. Rev. B **92**, 235401 (2015).

[23] G. Tosi, F. A. Mohiyaddin, V. Schmitt, S. Tenberg, R. Rahman, G. Klimeck, and A. Morello, Silicon quantum processor with robust long-distance qubit couplings, Nat. Commun. **8**, 450 (2017).

[24] H. J. Kimble, The quantum internet, Nature (London) **453**, 1023 (2008).

[25] M. J. A. Schuetz, E. M. Kessler, G. Giedke, L. M. K. Vandersypen, M. D. Lukin, and J. I. Cirac, Universal Quantum Transducers Based on Surface Acoustic Waves, Phys. Rev. X **5**, 031031 (2015).

[26] J. Majer, J. M. Chow, J. M. Gambetta, J. Koch, B. R. Johnson, J. A. Schreier, L. Frunzio, D. I. Schuster, A. A. Houck, A. Wallraff, A. Blais, M. H. Devoret, S. M. Girvin, and R. J. Schoelkopf, Coupling superconducting qubits via a cavity bus, Nature (London) **449**, 443 (2007).

[27] L. Childress, A. S. Sørensen, and M. D. Lukin, Mesoscopic cavity quantum electrodynamics with quantum dots, Phys. Rev. A **69**, 042302 (2004).

[28] G. Burkard and A. Imamoglu, Ultra-long-distance interaction between spin qubits, Phys. Rev. B **74**, 041307(R) (2006).

[29] V. Srinivasa, J. M. Taylor, and C. Tahan, Entangling distant resonant exchange qubits via circuit quantum electrodynamics, Phys. Rev. B **94**, 205421 (2016).

[30] G. Burkard, M. J. Gullans, X. Mi, and J. R. Petta, Superconductor–semiconductor hybrid-circuit quantum electrodynamics, Nat. Rev. Phys. **2**, 129 (2020).

[31] A. Cottet and T. Kontos, Spin Quantum Bit with Ferromagnetic Contacts for Circuit QED, Phys. Rev. Lett. **105**, 160502 (2010).

[32] N. Samkharadze, G. Zheng, N. Kalhor, D. Brousse, A. Sammak, U. C. Mendes, A. Blais, G. Scappucci, and L. M. K. Vandersypen, Strong spin-photon coupling in silicon, Science **359**, 1123 (2018).

[33] X. Mi, M. Benito, S. Putz, D. M. Zajac, J. M. Taylor, G. Burkard, and J. R. Petta, A coherent spin–photon interface in silicon, Nature (London) **555**, 599 (2018).

[34] F. Borjans, X. G. Croot, X. Mi, M. J. Gullans, and J. R. Petta, Resonant microwave-mediated interactions between distant electron spins, Nature (London) **577**, 195 (2020).

[35] P. Harvey-Collard, J. Dijkema, G. Zheng, A. Sammak, G. Scappucci, and L. M. K. Vandersypen, Coherent Spin-Spin Coupling Mediated by Virtual Microwave Photons, Phys. Rev. X **12**, 021026 (2022).

[36] M. Benito, J. R. Petta, and G. Burkard, Optimized cavity-mediated dispersive two-qubit gates between spin qubits, Phys. Rev. B **100**, 081412(R) (2019).

[37] A. Warren, E. Barnes, and S. E. Economou, Long-distance entangling gates between quantum dot spins mediated by a superconducting resonator, Phys. Rev. B **100**, 161303(R) (2019).

[38] C. Rigetti and M. Devoret, Fully microwave-tunable universal gates in superconducting qubits with linear couplings and fixed transition frequencies, Phys. Rev. B **81**, 134507 (2010).

[39] A. Warren, U. Güngördü, J. P. Kestner, E. Barnes, and S. E. Economou, Robust photon-mediated entangling gates between quantum dot spin qubits, Phys. Rev. B **104**, 115308 (2021).

[40] A. D. Córcoles, J. M. Gambetta, J. M. Chow, J. A. Smolin, M. Ware, J. Strand, B. L. T. Plourde, and M. Steffen, Process verification of two-qubit quantum gates by randomized benchmarking, Phys. Rev. A **87**, 030301(R) (2013).

[41] S. Sheldon, E. Magesan, J. M. Chow, and J. M. Gambetta, Procedure for systematically tuning up cross-talk in the cross-resonance gate, Phys. Rev. A **93**, 060302(R) (2016).

[42] N. Sundaresan, I. Lauer, E. Pritchett, E. Magesan, P. Jurcevic, and J. M. Gambetta, Reducing unitary and spectator errors in cross resonance with optimized rotary echoes, PRX Quantum **1**, 020318 (2020).

[43] P. Jurcevic, A. Javadi-Abhari, L. S. Bishop, I. Lauer, D. F. Bogorin, M. Brink, L. Capelluto, O. Günlük, T. Itoko, N. Kanazawa, A. Kandala, G. A. Keefe, K. Krsulich, W. Landers, E. P. Lewandowski, D. T. McClure, G. Nannicini, A. Narasgond, H. M. Nayfeh, E. Pritchett *et al.*, Demonstration of quantum volume 64 on a superconducting quantum computing system, Quantum Sci. Technol. **6**, 025020 (2021).

[44] M. Malekakhlagh and E. Magesan, Mitigating off-resonant error in the cross-resonance gate, Phys. Rev. A **105**, 012602 (2022).

[45] M. Russ, D. M. Zajac, A. J. Sigillito, F. Borjans, J. M. Taylor, J. R. Petta, and G. Burkard, High-fidelity quantum gates in Si/SiGe double quantum dots, Phys. Rev. B **97**, 085421 (2018).

[46] E. Kawakami, P. Scarlino, D. R. Ward, F. R. Braakman, D. E. Savage, M. G. Lagally, M. Friesen, S. N. Coppersmith, M. A. Eriksson, and L. M. K. Vandersypen, Electrical control of a long-lived spin qubit in a Si/SiGe quantum dot, Nat. Nanotechnol. **9**, 666 (2014).

[47] D. M. Zajac, A. J. Sigillito, M. Russ, F. Borjans, J. M. Taylor, G. Burkard, and J. R. Petta, Resonantly driven CNOT gate for electron spins, Science **359**, 439 (2018).

[48] T. Bonsen, P. Harvey-Collard, M. Russ, J. Dijkema, A. Sammak, G. Scappucci, and L. M. K. Vandersypen, Probing the Jaynes-Cummings Ladder with Spin Circuit Quantum Electrodynamics, Phys. Rev. Lett. **130**, 137001 (2023).

[49] M. A. Nielsen, A simple formula for the average gate fidelity of a quantum dynamical operation, Phys. Lett. A **303**, 249 (2002).

[50] C. Tahan and R. Joynt, Relaxation of excited spin, orbital, and valley qubit states in ideal silicon quantum dots, Phys. Rev. B **89**, 075302 (2014).

[51] B. Schumacher, Sending entanglement through noisy quantum channels, Phys. Rev. A **54**, 2614 (1996).

[52] V. O. Shkolnikov, R. Mauch, and G. Burkard, All-microwave holonomic control of an electron-nuclear two-qubit register in diamond, Phys. Rev. B **101**, 155306 (2020).

[53] A. J. Sigillito, M. J. Gullans, L. F. Edge, M. Borselli, and J. R. Petta, Coherent transfer of quantum information in a silicon double quantum dot using resonant SWAP gates, NPJ Quantum Inf. **5**, 110 (2019).

[54] P. Stano and D. Loss, Review of performance metrics of spin qubits in gated semiconducting nanostructures, Nat. Rev. Phys. **4**, 672 (2022).

[55] F. Ginzel, A. R. Mills, J. R. Petta, and G. Burkard, Spin shuttling in a silicon double quantum dot, Phys. Rev. B **102**, 195418 (2020).

[56] J. Preskill, Quantum computing in the NISQ era and beyond, Quantum **2**, 79 (2018).

[57] D. Deutsch, A. Ekert, R. Jozsa, C. Macchiavello, S. Popescu, and A. Sanpera, Quantum Privacy Amplification and the Security of Quantum Cryptography over Noisy Channels, Phys. Rev. Lett. **77**, 2818 (1996).

[58] H. Yan, Y. Zhong, H. S. Chang, A. Bienfait, M. H. Chou, C. R. Conner, É. Dumur, J. Grebel, R. G. Povey, and A. N. Cleland, Entanglement Purification and Protection in a Superconducting Quantum Network, Phys. Rev. Lett. **128**, 080504 (2022).